Studia Quaternaria, vol. 39, no. 2 (2022): 113–128 DOI: 10.24425/sq.2022.140887

DEFINING ROCK-FORMING COMPONENTS OF HOLOCENE FRESHWATER CARBONATES VIA UNIVARIATE STATISTICAL AND MIXTURE ANALYSIS OF COMPUTER TOMOGRAPHY DATA

Nour Nayef Hassan Alzoubi*, Janos Geiger, Sandor Gulyas

University of Szeged, Department of Geology, 2-6 Egyetem u., H-6722, Szeged, Hungary; e-mails: Nour Nayef Hassan Alzoubi nouralzoubi@geo.u-szeged.hu, János Geiger geostatisztika@gmail.com, Sandor Gulyas csigonc@gmail.com

** corresponding author*

Abstract:

Carbonate rocks are among the sedimentary systems which preserve information on the formation and diagenetic history expressed in its composition (distribution of its major rock-forming components (RFC). For estimating RFC proportions at the micro-scale, a simple counting of visible RFCs in thin sections using overlaid grids is a long-used, well-established technique. However, computer tomography (CT) analysis provides us with quantitative data in 3D at both the scale of the entire sample and a resolution defined by dimensions of the voxels at the micro-scale. The quantitative data expressed in Hounsfield units (HU) correlates with the density of RFCs. In this work statistical properties of CT-based data for selected freshwater carbonate samples from the Danube-Tisza Interfluve have been assessed using histograms and boxplots. Univariate statistical parameters characterize each sample. The maximum-likelihood method of mixture analysis has been adapted to recover and estimate the parameters of these subpopulations. Subpopulations have been defined in the form of overlapping intervals using statistical parameters gained (mean±2STD). Five major components have been defined: empty and partially or entirely filled pores by calcite, limestone micrite, dolomite micrite matrix and limonite saturated matrix.

Key words: CT data, mixture analysis, rock-forming components, freshwater carbonates.

Manuscript received 13 November 2021, accepted 14 February 2022

INTRODUCTION

The Danube-Tisza Interfluve (DTI) found in the central part of Hungary is covered by wind-blown sand and loess deposits bearing dolomite and other carbonate minerals and having a carbonate content of up to 10%. Prevailing winds during the Late Pleistocene and the Holocene arranged these sands into a series of dunes of NW-SE direction (Miháltz, 1947, 1953; Molnár, 1961, 1970, 1988, 2000). Inter-dune depressions harbored some 150–200 alkaline freshwater lakes preceding river regulations of the 19th century (Fig. 1b). These lakes obtain their water from groundwater, rich in dissolved Ca and Mg, and surface runoff from the nearby areas (Molnár and Szónoky, 1976; Molnár and Murvai, 1976; Molnár *et al.,* 1995). Extensive freshwater carbonate strata composed of dolomitic limestone and dolomite developed during the Holocene (Miháltz and Faragó, 1946; Miháltz, 1947, 1953; Mucsi, 1963; Molnár, 1961, 1970, 1980, 1983, 1985; Jenei *et al*., 2007; Sümegi *et al*., 2015a, b). In general, two basic types of carbonate strata are present in the area with loose carbonate muds, 30–110 cm thick, overlying loess or wind-blown sands being restricted to the northwestern part. In the southeast where the lacustrine phase of carbonate formation ended, diagenesis allowed for the formation of solid carbonate rock (dolomitic limestone), overlain by unlithified carbonate muds in its upper parts (Miháltz 1947, 1953; Miháltz and Faragó, 1946; Molnár, 1961, 1970, 1980, 1983, 1985; Jenei *et al.,* 2007; Mucsi, 1963; Sümegi *et al*., 2015a, b). The precipitation of high magnesium calcite from the lake water, and the formation of dolomite and proto-dolomite attributable to seasonal variations of the climate and concomitant volume, geochemical (pH, dissolved element concentration) changes of the groundwater, pore waters and the water body in these lacustrine environments is a unique feature of the area. The formation of freshwater carbonates in the freshwater lakes of the DTI has been discussed in various studies (Miháltz 1947, 1953; Miháltz and Faragó, 1946; Molnár, 1961, 1970, 1980, 1983, 1985; Mucsi, 1963; Müller, 1970; Müller *et al*., 1972; Jenei *et al*., 2007; Sümegi *et al*., 2015a, b). Müller *et al.* (1972) presented a general model of lacustrine carbonate formation using data from 25 European and Anatolian lakes of varying salinity and

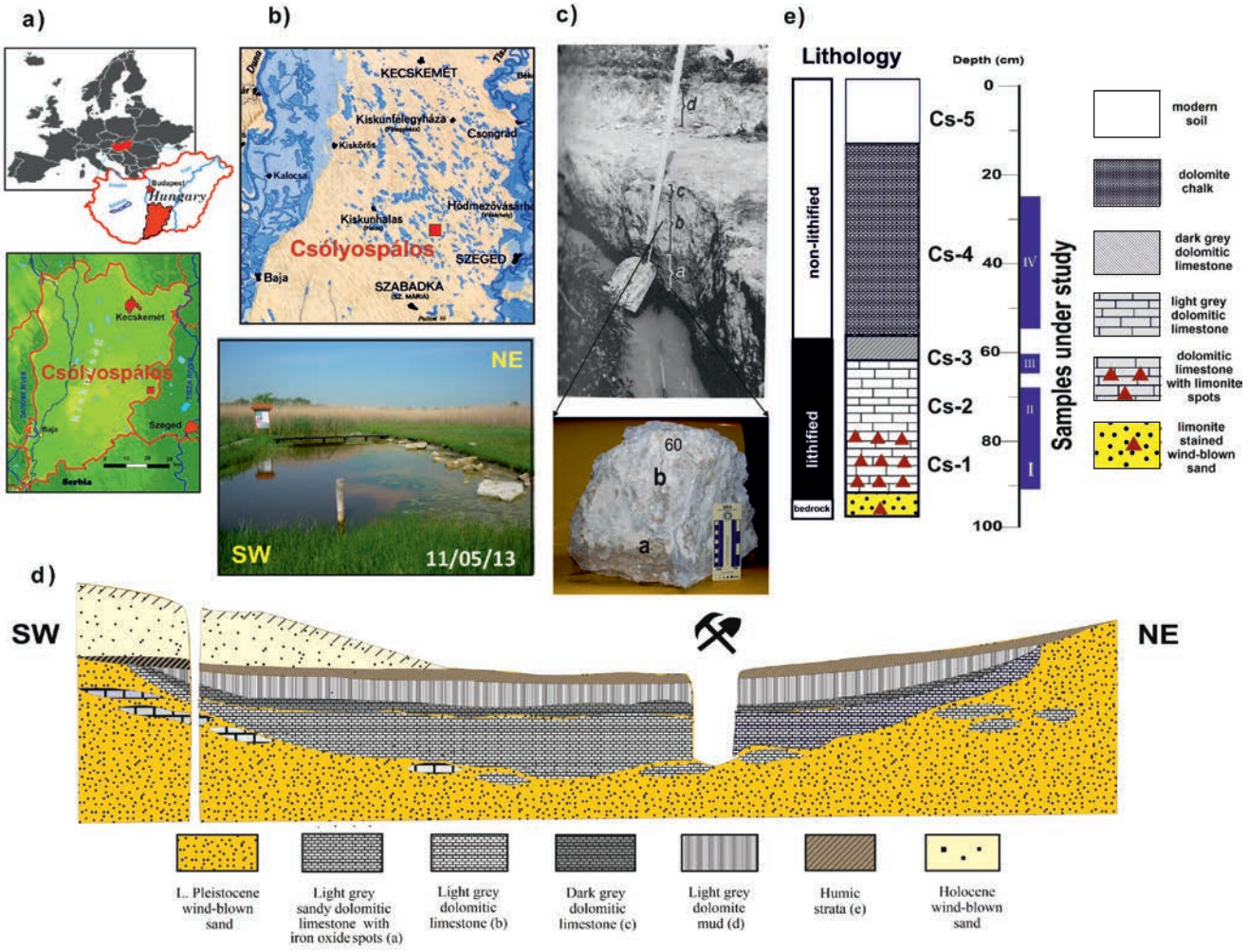

Fig. 1. Location and stratigraphy of the studied carbonate sequence at the site of Csólyospálos. (a. location, b. hydrography of the area before the late 19th century, c. photograph of the 1970 profile by Molnár with his names of the lithological members, d. geological cross-section of the site and view of the outcrop during early spring e. detailed lithology of the outcrop with the position of samples under study marked).

hydrochemistry. Temperature, pH and ion concentrations are the main factors that control the type of carbonate minerals that are be formed. The precipitation of primary carbonates (calcite, high-Mg calcite, aragonite, hydrous Mg carbonate) and secondary carbonates (proto-dolomite, dolomite, huntite, magnesite) depend on the Mg/Ca ratio of the lake and pore waters. Secondary carbonates along with high-Mg calcite appear in lakes where the mentioned ratio is >7, a total water salinity is high and changes significantly during a year. Although the definition of the proto-dolomite is not fully settled yet in carbonate sedimentology (Müller, 1970; Gaines, 1977; Fang and Xu, 2019), the proto-dolomite is considered to be a mineral where the composition approaches that of the dolomite mineral, yet only a partial structuring of Ca^{+2} and Mg^{+2} is notable in its lattice (Müller and Wagner, 1978; Tullner and Cserny, 2003; Chen *et al*., 2017).

Proto-dolomite forms in a mud deposited on a lake bed *via* a transformation of Mg-bearing calcite during periods when pore waters are especially rich in Mg (Müller *et al*., 1972; Gaines, 1977; Müller and Wagner, 1978; Fang and Xu, 2019). Such conditions generally emerge during the fall in the ponds of the DTI. The total dissolved solids content (TDS) of the groundwaters of the DTI is relatively high (500–2000 mg/l in general, sometimes >5000 mg/l). Due to high summer temperatures and minimal rainfall, strong evaporation reduces the lake levels. As the lost water is recharged from the groundwater, the TDS of the lake water further increases to values between 8000–70,000 mg/l, turning these ponds highly saline (Molnár and Murvai, 1976; Molnár and Szónoky, 1976; Molnár *et al*., 1995; Molnár, 1996). From the ions present, sodium is dominant in addition to calcium, magnesium, and hydro-carbonate making the water highly alkaline with pH ranging between 9–11. Groundwater also drops to 3–8 m depth and many of the lakes dry up by the end of summer (Molnár, 1991).

Precipitation during the fall brings in freshwater reducing salinity, and the concentration of Na and K allowing for an increase in Mg/Ca ratio to values between 7–12, leading to the precipitation of high magnesium calcite (Molnár, 1961, 1970, 1981, 1983, 2015; Bender *et al*., 1975). As a result, the Mg/Ca ratio further increases in the remaining pore waters bringing about the early diagenetic alteration of the high magnesium calcite into a proto-dolomite (Mucsi, 1963; Molnár, 1970, 1980, 1983, 1985, 1991). As the ratio

of CO_3/Ca is higher than 1, these conditions also favor the formation of dolomite. Where the lacustrine phase of carbonate precipitation ended, seasonal migration of the pore waters saturates the matrix and fills up the pores with minerals precipitating from the remaining solution (calcite, limonite), turning the carbonate mud into solid rock. Due to the smaller Mg/Ca ratio attributable to the exhaustion of magnesium during the proto-dolomite, dolomite formation and reduced salinity of the pore waters, the pore-filling cement is calcitic in composition (Molnár, 1970, 1980, 1983, 1985, 1991). Thus, in the freshwater carbonates of the DTI, the precipitation of the carbonate matrix reflects the evolution of the lacustrine system itself, while the formation of the carbonate cement infilling the pores is a secondary process carrying information on the diagenesis.

The formation and diagenetic history of sedimentary rocks is expressed in their composition that is distribution of its major rock-forming components (RFC). To understand, assess the nature of these processes and resulting spatial heterogeneity, one needs quantitative information on the distribution of RFCs at the macro and micro-scale.

Analysis of texture characters of carbonate sedimentary rocks of the interfluve area has been extensively studied both at the macro (hand specimen) and micro-scale (thin sections) (Molnár, 1961, 1970, 1980, 1983, 1985, 1991, 1996; Mucsi, 1963; Molnár and Murvai 1976; Molnár and Szónoky, 1976; Molnár *et al*., 1995). For estimating RFC proportions at the micro-scale, a simple counting of visible RFCs in thin sections using overlaid grids is a long-used, well-established technique. The quantitative information gained in this way has certain limitations though. Firstly, it is two-dimensional, spatially heavily restricted representing only a minor fragment of the entire sample; i.e. the scale of the area covered by the thin sections. In addition, estimations are rather subjective. Several different RFCs are present within a single grid cell, so correct filtering of the individual components and estimation of their proportions in the grid is not without a bias. Computer Tomography (CT) analysis however provides us quantitative data in 3D at both the scale of the entire sample and a resolution defined by dimensions of the voxels in the micro-scale. The quantitative data expressed in Hounsfield units (HU) correlates with the density of RFCs. Thus, its statistical properties also record information on their heterogeneity. This work presents results of a detailed quantitative analysis of data gained via CT analysis.

GEOLOGY AND STRATIGRAPHY

The DTI forms a wind-blown sand and loess-covered ridge (180 km long and 120 km wide, 100–150 m a.s.l.) between the Danube and Tisza rivers in central of Hungary (Fig. 1a). To the west, the area is bordered by the tectonic depression of the Danube valley lying at 90–100) m a.s.l. The 10–15 km wide valley of the Tisza River (80 m a.s.l.) forms the eastern boundary of the area. The bedrock of the DTI is given by alternating loess and wind-blown sand sequences representing the reworked fluvial deposits of the Danube.

During the Holocene prevailing winds arranged the sand into a series of dunes with an NW to SE trend. The interdune depressions are occupied by natron lakes characterized by freshwater carbonate formation, supplied with water primarily from groundwater flowing from the Danube valley in the west towards the Tisza valley in the east (Fig. 1b) (Molnár and Murvai 1976; Molnár and Szónoky, 1976; Molnár *et al*., 1995). Our study site at Csólyospálos located on the southeastern side of the DTI (Fig. 1a, b) represents one of such interdune lacustrine systems where carbonate formation starting at the beginning of the Holocene came to an end about 3500 years ago (Jenei *et al*., 2007; Sümegi *et al*., 2015a, b). The outcrop is situated ca. 2 km northeast of the village of Csólyospálos at 92 m a.s.l. A geological profile created in the centre of the Late Pleistocene interdune depression exposes a ca. 1 m thick carbonate sequence covered by the Late Holocene black earth soils. The former pond is flanked by the Holocene dune in the SE (Fig. 1c, d). The carbonate sequence overlying the bedrock of the Late Pleistocene wind-blown sand is comprised of a lower lithified and an upper non-lithified part. Based on its observed lithological features the sequence was subdivided into 5 members (Fig. 1c, e) (Molnár, 1961, 1970, 1980, 1983).

The member Cs-1 (corresponds to the Molnar's member A) is a sandy dolomitic limestone of looser structure with vertical veins stained by red limonite. It is 20–30 cm thick. This unit transforms into the member Cs-2 (corresponds to the Molnar's member B), with no clear boundary at the top. Cs-2 is a solid light-grey dolomitic limestone, 30–40 cm thick with vertical vugs of several cm corresponding to roots of the former aquatic vegetation, hence its folk name is honeycomb stone. There is a sharp lithological boundary between the member Cs-2 and the overlying member Cs-3 (corresponds to the Molnar's member C). Cs-3 is a solid dark-grey dolomitic limestone, 5–8 cm thick, with the highest carbonate content in the entire sequence (>80%). Here vuggy and moldic type porosity is present in a form of shelter, gas pores and desiccation or sheet cracks in addition to vugs corresponding roots of a former vegetation. In some pores, the intrusion of not fully consolidated carbonate mud is also visible. Most of the pores are partially or completely infilled by calcisparits. Pore filling starts perpendicularly to the pore wall forming pore-lining structures. The member Cs-4 (corresponds to the Molnar's member D) is the last carbonate member with an average thickness of 30–60 cm. In contrast to the previous members, Cs-4 is non-cemented with carbonate mud of bright white colour. The highest volume of unfilled pores, as well as carbonate clastic grains, appear here. The carbonate content is about 50–60%.

Based on textural analyses implemented using thin sections, the carbonates are wackestone type with a mud-supported texture. Rock-forming components are dominantly micrite (~69%), quartz and feldspar grains (~13.6%), unfilled pores (to ~12%), carbonate lithics (~3%) and microsite sparite infilling pores (2.4%). Shells of freshwater gastropods and oogonia of calcareous algae are also present in

minimal proportions similarly to additional contaminants of iron oxides, manganese, fine organic and clay particles (Molnár, 1961, 1970, 1980, 1983, 1985, 1991, 1996; Molnár and Murvai 1976; Molnár and Szónoky, 1976). The density of the rock ranges between 2.729 and 2.790 g/cm^3, with porosities of 25.77–29.82% (Mucsi, 1963), depending on dolomite and iron-oxides, manganese content as well as the cementation degree.

MATERIAL AND METHODS

Computer Tomography

X-ray CT imaging is a non-destructive examination technique, based on measuring the penetrating radiation intensities over several paths of a sample to produce cross-sectional tomographic views based on density differences. The first use of CT was for medical purposes (Kenter, 1989), then it has been widely used in various sciences as archaeology, palaeontology and sedimentology (Földes *et al*., 2004; Markussen *et al*., 2019). The CT technique was used in the early 1980s for scanning meteorites, detecting soil porosity and analysing sediment morphology. Moreover, the CT technique was employed in palaeontology to scan the irreplaceable fossils in the mid-1980s (Cnudde *et al*., 2006). Later on, the same technique was used in detecting rock-faulting by the early 1990s. Recently, the micro-CT method was employed first in a laboratory experiment related to structural geology in 2000.

In general, the CT technique is highly sensitive to density changes or any variation in chemical, physical or biological properties of materials (Maurício *et al*., 2017). For this reason, post- or syndiagenetic sedimentary structures can be easily detected visually on CT scans (Wilding *et al*., 2005). Thus, this technique is widely used in studies of clastic rocks. However, a limited number of works have been conducted on carbonates (Hicks *et al*., 1994). The most important feature of the CT analysis, besides visual evaluation, is however the data behind, which carries quantitative information on density differences observed between rock-forming textural components in a material. These can be thus assessed using various statistical approaches (De Boever *et al*., 2015).

The CT measurements were performed on 4 samples representing all members of the carbonate sequence of Csólyospálos (Cs-1, Cs-2, Cs-3, Cs-4, and Cs-5), using the Siemens Emotion 6 medical scanner at the Department of Radiology, University of Pécs, Hungary. A single sample (sample I) represents the members Cs-1 and Cs-2. Two adjacent samples (sample II and III) were taken from the member Cs-3 and an additional single sample (sample IV) represents the member Cs-4 (Fig. 1). The CT instrument operates at 140 kVp (peak kilovoltage), with 189 mAs (milliampere-seconds) current and 1.5 s exposure time. The lateral resolution was 0.23 × 0.23 mm^2, with 1.5 mm of scan-layer thickness. The CT images have been exported as DICOM. A 3D volume rendering software was used for visualization, filtering and data extraction. Details on Field of View (FOV) for each sample and the representative voxel sizes are presented (Table 1).

Table 1. List of samples with Field of view (FOV) for the entire sample and representative voxel size parameter.

Samples with stratigraphic position	FOV (mm)	Voxel size (mm^3)
I	669,866	0.08
(Members Cs-1, Cs-2)	(95.5*22.7*309)	
II	305,375	0.08
(Member Cs3)	(79.5 *132 *29.1)	
III	175,882	0.04
(Member Cs-3)	(138*23.3*54.7)	
IV	518,583	0.08
(Member Cs-4)	(76*159.8*42.7)	

The workflow applied

The visual output of computed tomography allows for straightforward interpretation *via* comparison with the original sample and the available macroscopic lithological descriptions (Fig. 2). However, certain scanning artifacts like beam hardening can obscure details of interest or cause the CT value of a single material to change in different parts of an image. To overcome this problem the outer part of the image has been removed creating a CT brick (subset) smaller in volume than the original sample (filtering) (Fig. 2). Thus, only the created central sub-volume of the original sample was used for further visual and quantitative analyses.

Data extracted from the brick were used in further statistical analysis using the software packages Statigraphics and Past 4.06 (Hammer *et al*., 2001). Distribution types were visually assessed using histograms and boxplots to identify potential outliers and extreme values present in the samples (Fig. 2).

Univariate statistical parameters (mean, standard deviation, skewness, kurtosis) have been used to characterize each sample. As our samples assumed to represent a pool of normally distributed populations corresponding to the rock-forming components, the maximum-likelihood method of mixture analysis has been adopted to recover and estimate the parameters of two or more univariate normal distributions (Mean, STD) in Past 4.06 (Fig. 2). The method is based on the end member (EM) algorithm of Dempster *et al.* (1977). To see if the number of groups chosen is appropriate and avoid overfitting, the Akaike Information Criterion (AIC; Akaike, 1974; Hammer *et al*., 2001) is calculated. Each data point has been assigned to one of the groups using a maximum likelihood approach. This can be used as a non-hierarchical clustering method for univariate data.

The statistical parameters gained for each subpopulation have been used to set HU value intervals. Using the gained parameters of the mean ± and 2 STD, the recovered subpopulations are visualized and their lithological meaning is assessed relying on the descriptive geological reports and thin

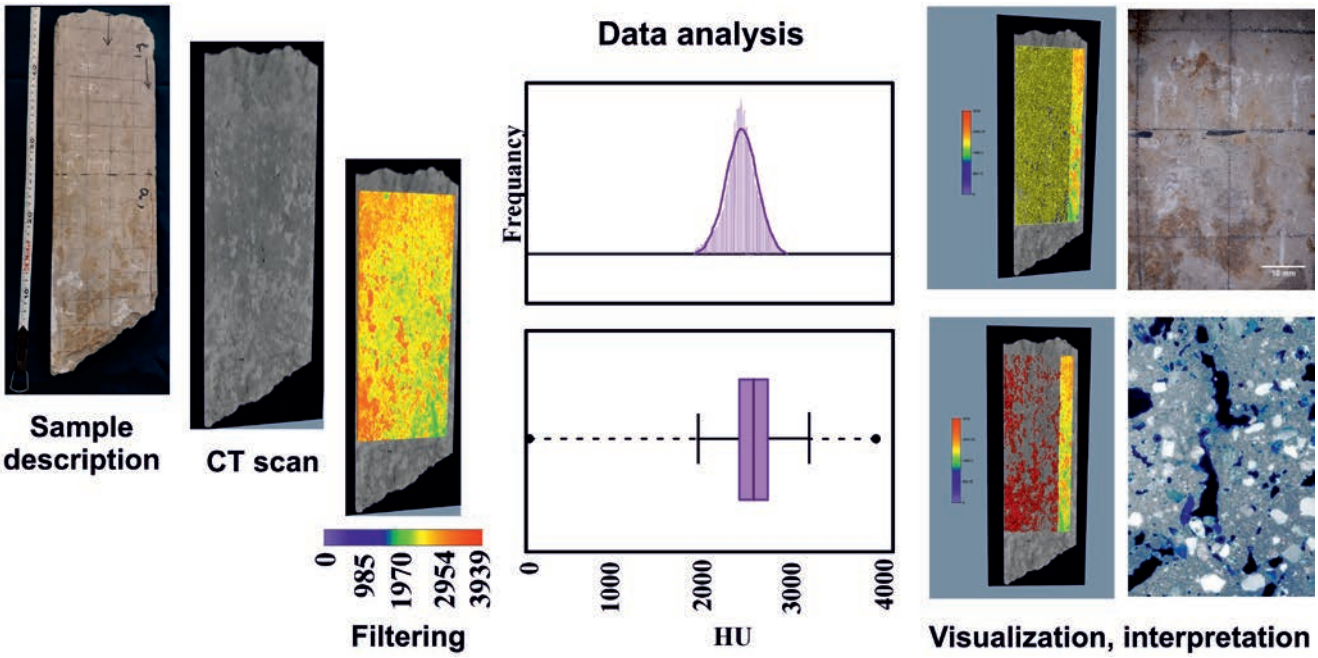

Fig. 2. The general presentation of the workflow.

sections of Molnár *et al.* (1976) and Molnár (1980, 1981). HU intervals set for each meaningful sub-populations using the referred statistical parameters can be regarded to quantitatively describe rock-forming components present in the samples. Knowing the original volume of the studied and filtered subsamples, the percentage of each identified rock-forming component (e.g., calcitic matrix, filled pores, etc.) can also be estimated. The proportions of each rock-forming component calculated can be compared to those defined by Molnár *et al.* (1976) and Molnár (1980, 1981, 1991), based on multiple thin sections taken from selected parts of the samples.

However, the adoption of quantitative CT analysis and 3D visualization has several significant advantages over the traditional approaches of Molnár *et al.* (1976) and Molnár (1980, 1981, 1991). Thin section analysis allows for the characterization of a very small volume of the sample. Furthermore, even if multiple thin sections are prepared, they capture only a very small part of the entire block sample. In contrast in the CT analysis, the percentage and spatial distribution of each rock-forming component can be assessed for the entire CT brick allowing to reveal small-scale vertical and horizontal heterogeneity present.

RESULTS

Sample I, members Cs-1 and Cs-2

The sample HU values follow an univariate, slightly negatively skewed leptokurtic distribution (MD: 2560, STD: 255, SK: -1.4, K: 9.3). The single peak with the value of 2382 HU is close to the mean value of the sample, reflecting the general dominance of a single rock-forming component (matrix) (Fig. 3). Based on results of the mixture analysis 5, overlapping intervals can be distinguished with densities ranging between 0 and 3939 HU (Fig. 3). The group A has values lower than 626 HU. The group B has values between 277 to 2245 HU. Both groups appear as outlier and extreme values on the boxplot.

When we look at the shape, structure and spatial distribution of the rock-forming components characterized by these intervals, they appear as isolated or interconnected longitudinal tubular or spherical, lenticular structures on the 3D CT brick (Fig. 4).

When compared with the original sample photos, general textural descriptions of Molnár (1981, 1983, 2015) as well as photos of thin sections (Fig. 4), these must correspond to the pores present in the sample. According to Molnár (1981, 1983), most of the pores are vugs, intergranular and moldic pores. Vugs corresponding to roots of the former vegetation appear in various forms and orientation. These connected or isolated tubes are either scattered in the matrix independently of lamination or cross-cut bedding planes. Horizontal desiccation pores also turn up in addition to randomly scattered gas pores. Some pores are empty while others are partially filled by calcite sparite or microsparite. These are also clearly visible on the enlarged photo of the middle part of the sample and the thin sections (Fig. 4). The group A corresponding to the values 0–626 HU thus represents the empty pores, while that of 277–2245 HU (group B) corresponds to the pores partially filled by calcite due to diagenetic processes (Fig. 4). As seen in the lower left figure (Fig. 4), a spiral-like structure also turns up (G) corresponding to the shell of an aquatic gastropod. Pore lining calcite crystals are common in empty gastropod shells, in addition to matrix intrusions (Fig. 4).

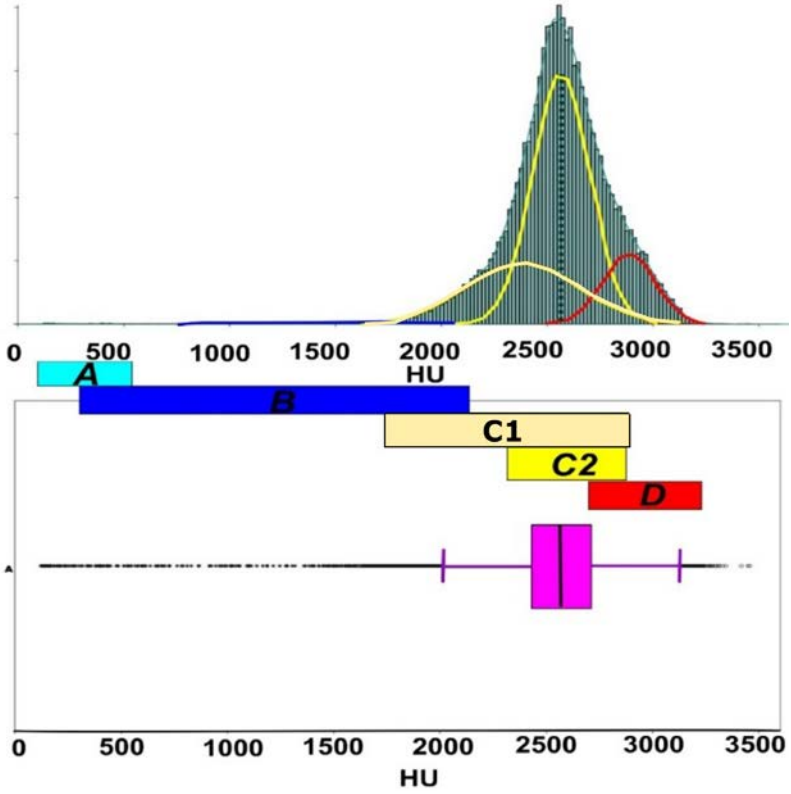

Fig. 3. Statistical characteristics of sample I and revealed subpopulations (A, B, C1, C2, D) represented by overlapping normal distribution curves on the frequency histogram.

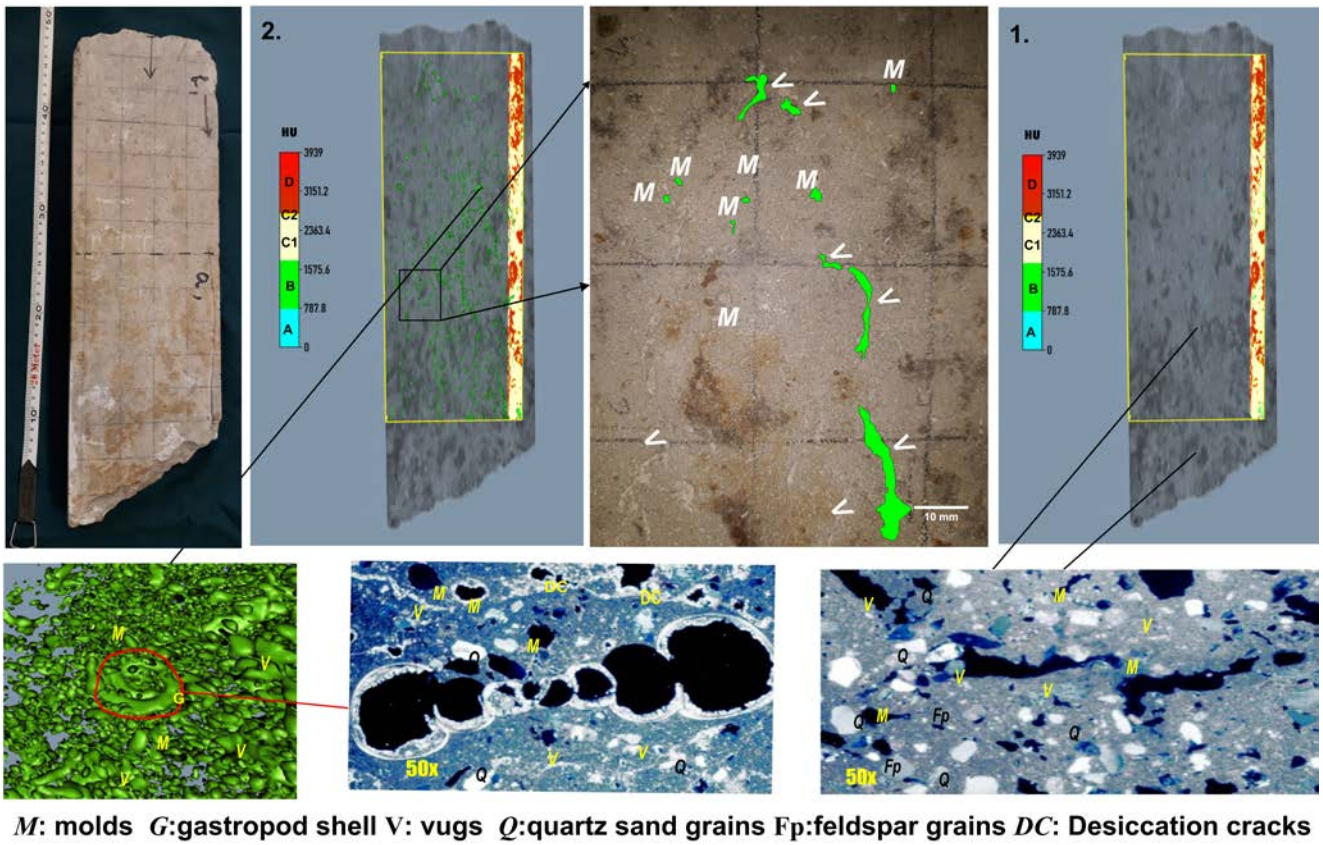

Fig. 4. The visual appearance of group A (1) and B (2) on the CT blocks of sample I and examples of corresponding textural components depicted on sample photos (center) and selected thin sections.

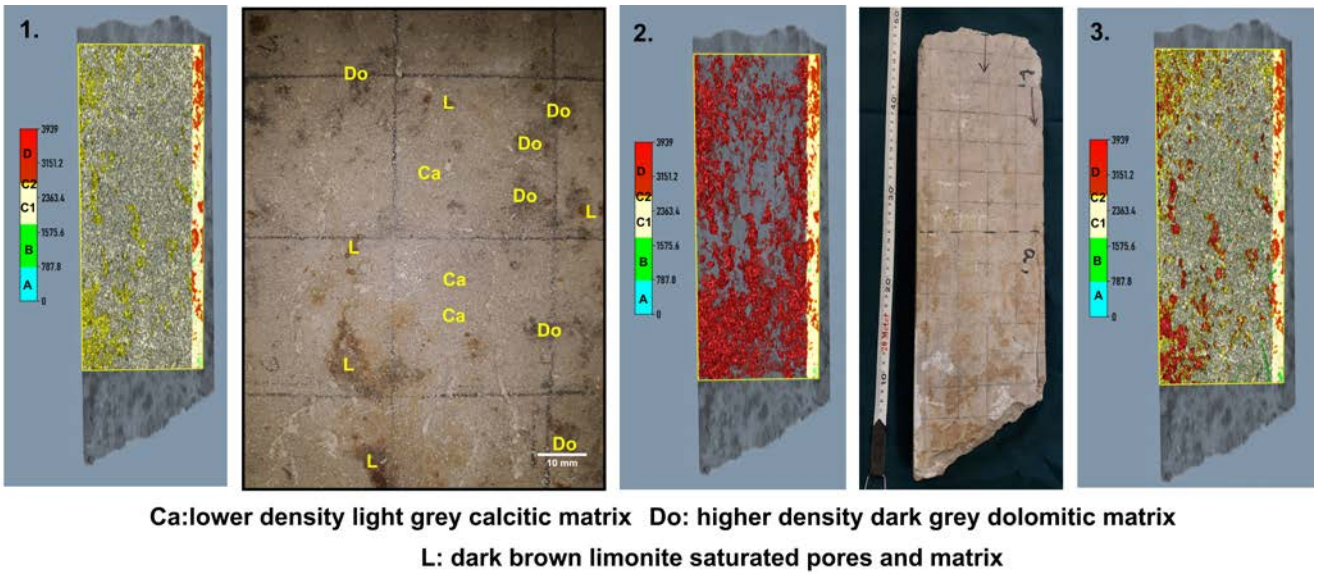

Fig. 5. The visual appearance of HU intervals of group C1, C2, and D on the CT block of sample I (1,2), combined visualization of the matrix (C), and the highest density limonite saturated matrix components (D) (3).

The group C with values between 1900–3125 HU gives ca. 75% of the sample (IQR + whiskers of the boxplot) and can be divided into two subgroups (Fig. 3), with a lower (C_1: 1869–2896 HU) and higher density (C2: 2299–2832 HU). As the dominant component of the sample is the micrite, C_1 and C_2 must correspond to the matrix with differing densities. The group C_1 overlaps with the group B, which we interpreted as the calcitic fill of the pores. This way, C_1 must correspond to the dominantly calcitic matrix. Consequently, C_2 must correspond to the matrix composed of dominantly higher density minerals (dolomite micrite). The group D is defined by values between approximately 2500 to 3500 HU, showing the highest density component in the sample appearing as the upper outlier on the boxplot (Fig. 3). Morphology, orientation and spatial distribution of the features defined by the mentioned D interval are very much like those defined by the intervals A and B (pores), displaying lenticular and vertical tubular structures running parallel to one another (Fig. 5/2). This material appearing as dark-brown spots on the sample photo representing the limonite saturated matrix (Fig. 5), probably formed as a precipitate in the pores and the matrix during the diagenesis phase.

Samples of the member Cs-3

Sample II

The sample HU values follow a bimodal slightly negatively skewed distribution (MD: 2787.3 HU, STD: 334.23, SK: -1.421, K: 2.365) with a marked peak at 3150 and a shoulder at 2750 HU reflecting the dominance of a high-density and a mid-density component, the latter being close to the sample mean (Fig. 6).

According to the results of mixture analysis, five overlapping groups could have been differentiated in the sample, characterized by a relatively wide range of densities between 0 and 3500 HU (Fig. 6). The group A has values lower than 1386 HU. The group B has a wider distribution with values between 1387 and 2749 HU (Fig. 6). If we visualize the RFCs corresponding to these intervals on the CT brick, they appear to form a network of interconnected and isolated spherical and tubular structures (Fig. 7/1, 2). Based on their shape, they may represent various types of pores. As seen on the thin section and the surface photo of the sample (Figs. 7, 8), two types of pores are present: molds and vugs. Molds turn up as spherical elongated isolated structures in the brick for the defined interval. In addition, you can see long tubular structures, some of them being isolated, others being interconnected. These probably correspond to vugs. In addition, both molds and vugs can be further divided into two subgroups: relatively empty ones (Figs. 7, 8) and the other ones which are fully or partially filled with secondary calcite crystals, and in some cases by the matrix material. Filled pores appear as red-stained crystals on the Na alizarine sulphonate dyed thin sections (Fig. 8) and as white crystals on the surface photo of the sample.

It is also visible on thin sections that some crystals form pore-lining structures. When values for the group B are visualized essentially, the same morphologies and orientation appear as in the case of the group A (Fig. 7/1, 2). Based on the previously mentioned information, both groups A and B correspond to pores in the sample, the denser one (B) most likely indicates the presence of additional minerals, besides air-so partially or filled pores.

The figure in the upper left corner (Fig. 8) depicts a close-up view of the CT brick of the sample II. Here the marginal areas of the vugs found in the upper centre, upper right and right centre have values corresponding to the group

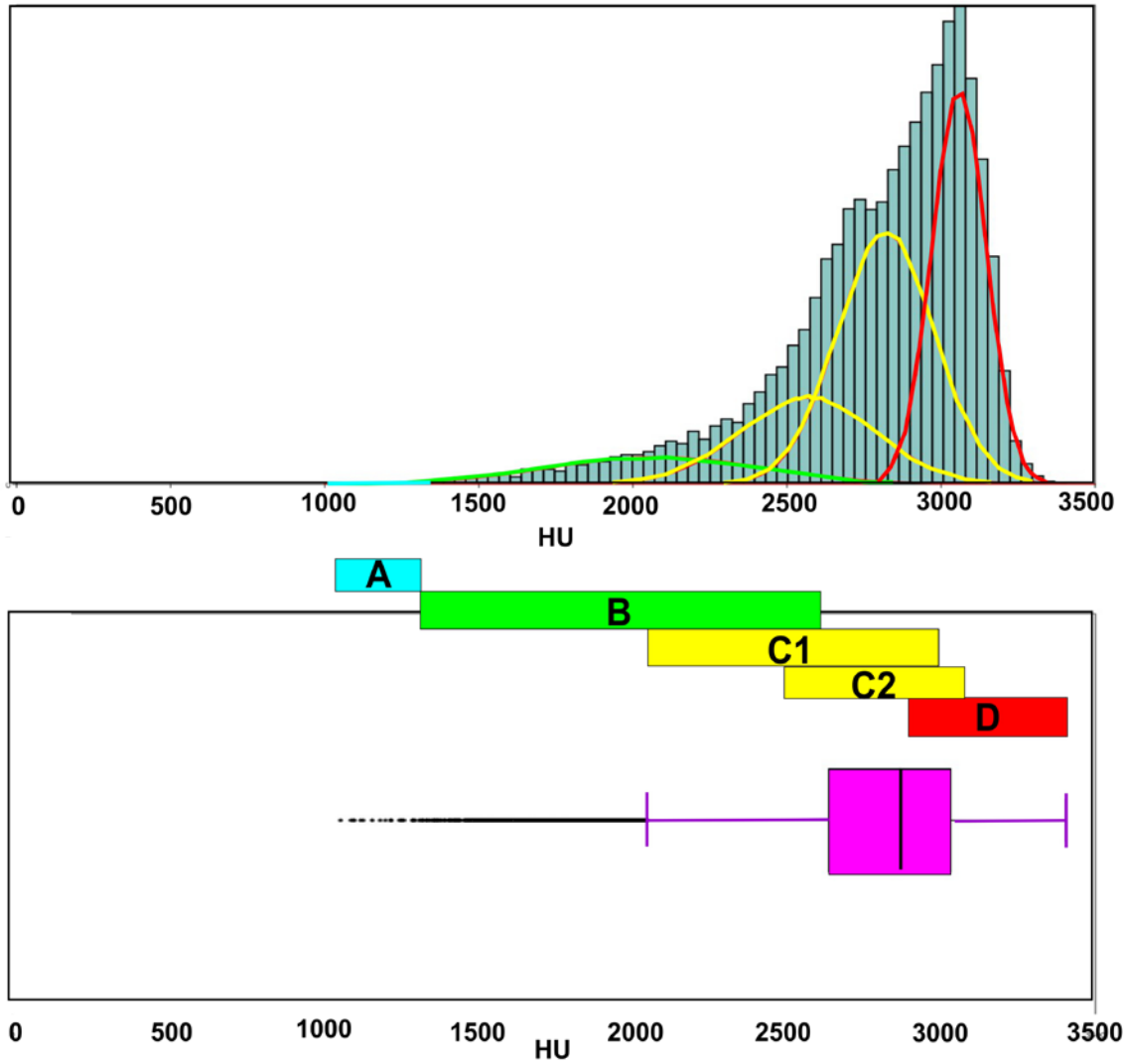

Fig. 6. Statistical characteristics of sample II revealed subpopulations (A, B, C1, C2, D) represented by overlapping normal distribution curves on the frequency histogram.

B. These must represent pore-lining calcite crystals. The middle part of these vugs, though with values corresponding to the group A, represents parts with the least dense component. Similar structures appear along the central line of the surface sample depicted on the upper right photo (Fig. 8), where the marginal areas of the vugs have white crystals and the central part is empty. There are other tubular or spherical structures as well, with values corresponding to the group B. These again can be interpreted as pores filled by higher density calcite crystals. All these observations further corroborate our previous interpretation that these two components (A, B) should represent the empty and partially filled areas of pores. Molds are not evenly spread in the brick but appear in higher densities in the top part (Figs. 7, 8). Vugs are also scattered, most of them being restricted again to the top part (Fig. 8) and in some cases, the lower left part of the CT brick (Figs. 7, 8). The orientation of the vugs is dominated by vertical crosscutting laminae.

The third group (Fig. 6C) corresponds to the interquartile area on the boxplot, indicating that this group gives a major part of the rock-forming components; i.e., the micritic matrix. The group C is characterized by two overlapping modes (C_1, C_2) indicating presence of two micritic components with different densities: a lower (group C_1: 2117–3001 HU) and a higher (group C_2: 2501 HU and 3136) ones. The material covers most of the sample (Fig. 7/3), indicating that the major component is a carbonate matrix composed of lower density calcitic micrite and higher density dolomitic micrite, appearing in the figure in light yellow and dark-yellow colour.

The last group (D) has the highest density values in the sample (2884–3235 HU). We can extend the upper boundary of this interval to the maximum value of the sample (3404 HU). Due to the overlap of the group D with the group C, which we interpreted as the matrix, this group must also represent a part of the matrix, where the presence of an even higher density material must be assumed. When the group D is visualized on the CT brick, this part of the sample corresponds to the dark grey-brownish lower part (Figs. 7, 8), representing a geochemical front (GF) where precipitates of dark-brown limonite and dark-grey dolomite stain the rock.

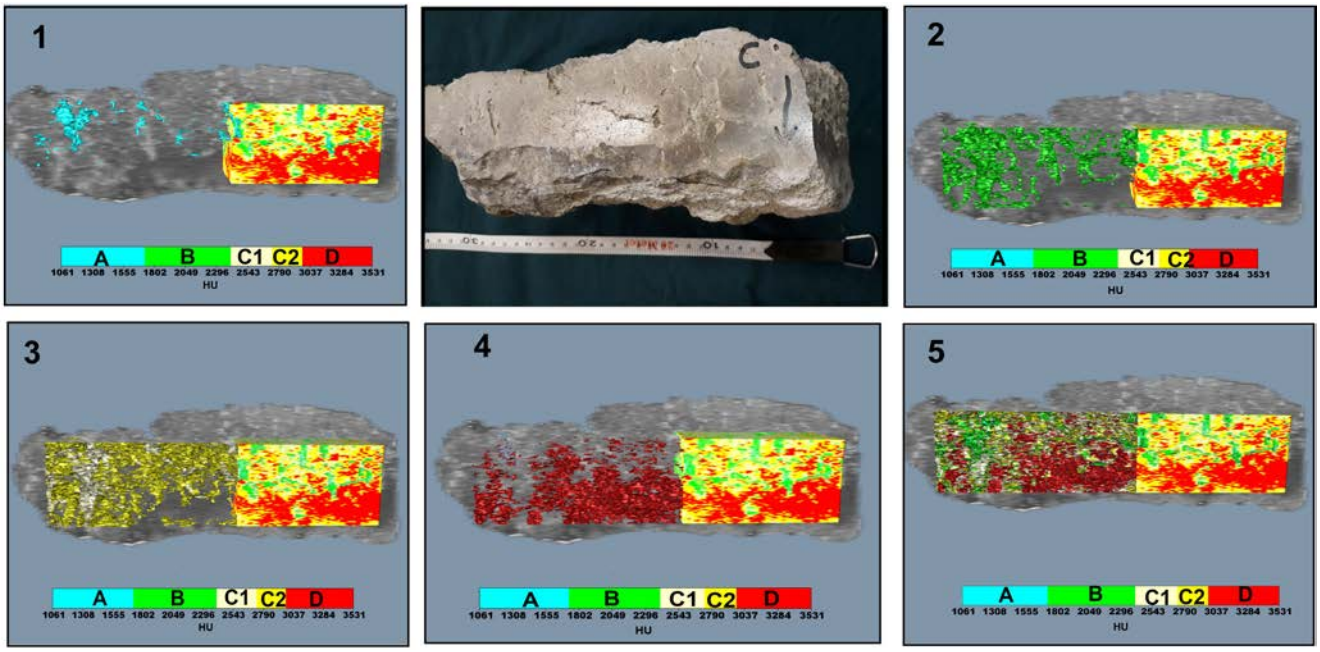

Fig. 7. The visual appearance of identified subpopulations (A, B, C1, C2, D) on the CT block of sample II (1: empty pores (A), 2: calcite-filled pores (B), 3. C1: matrix of dominantly calcite micrite, C2: matrix of dominantly dolomite micrite, 4: limonite and manganese saturated micrite (D) 5. combined textural components).

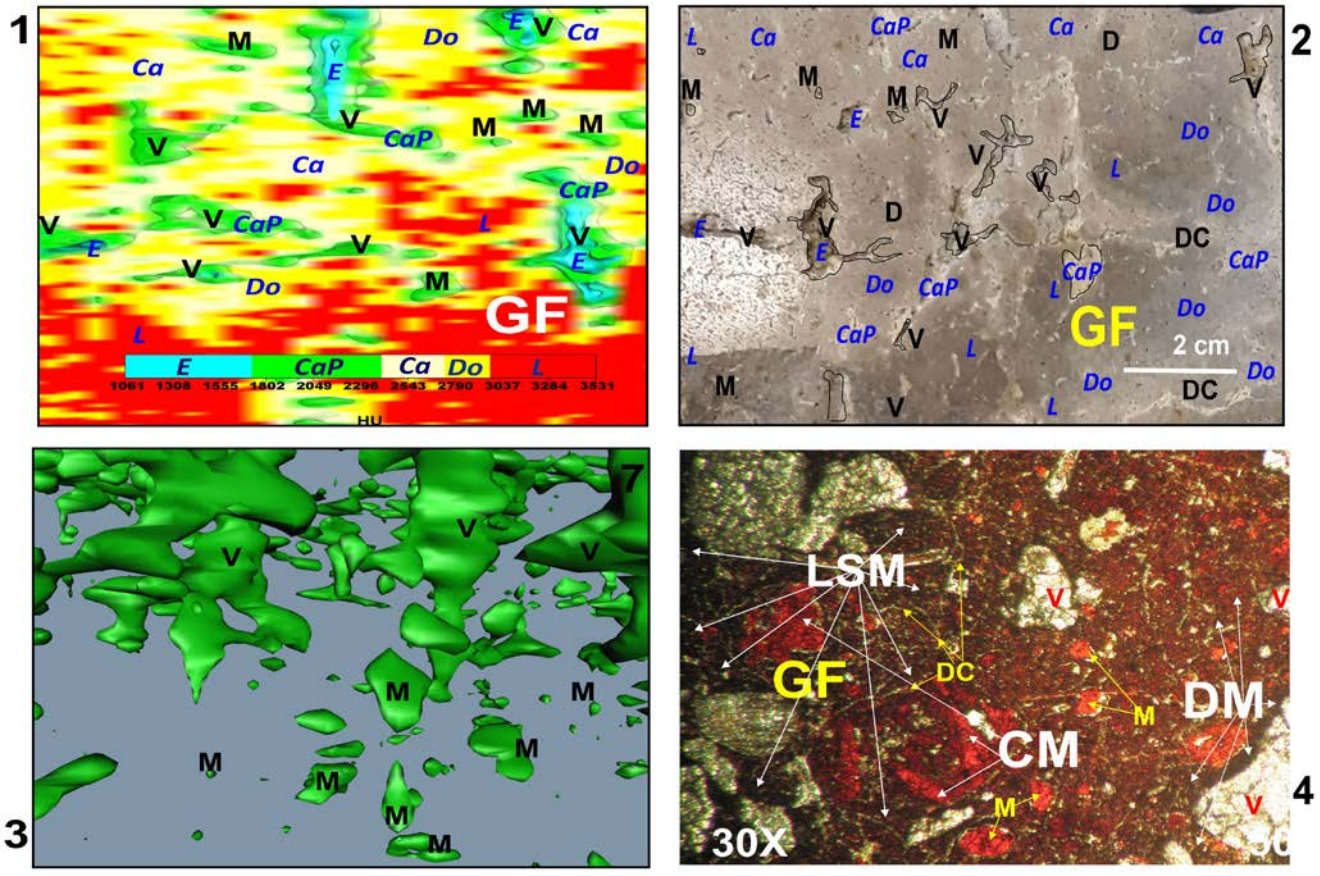

Fig. 8. Close-up view of sample II with different macro and micropores depicted on the CT block (1,3), sample surface (2), and under the microscope (4). (E: empty pores, Cap: calcite filled pores, Ca: matrix of dominantly calcite micrite, Do: matrix of dominantly dolomite micrite, L: limonite and manganese saturated micrite, pore Types-V: vugs (plant roots, plant stems), DC: desiccation cracks, M: molds (gas pores).

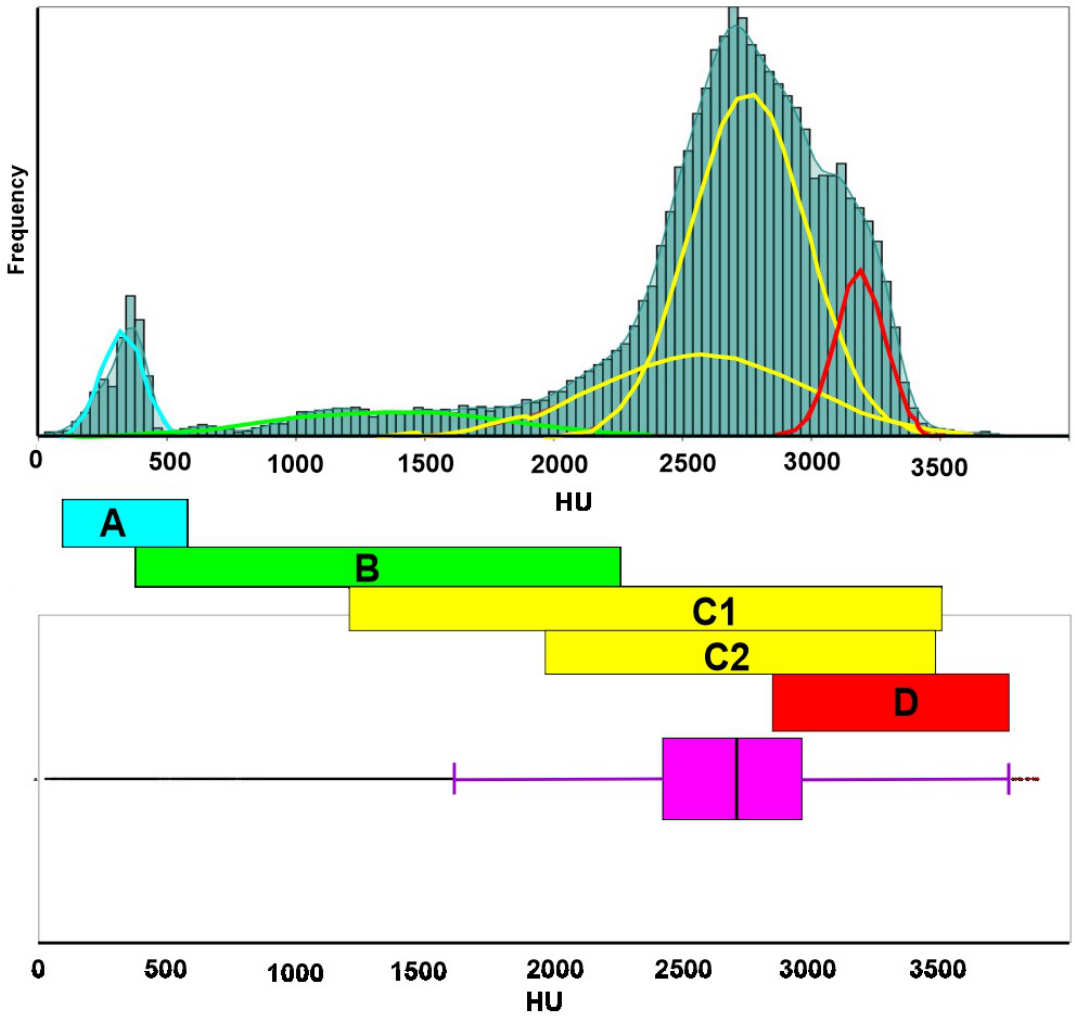

Fig. 9. Statistical characteristics of sample III and revealed subpopulations (A, B, C1, C2, D) represented by overlapping normal distribution curves on the frequency histogram.

It is interesting to note that in some places of the geochemical front, the limonite stained micritic matrix (L-red) is surrounded by the dark-grey dolomitic matrix (Do: dark-yellow). The light grey calcitic matrix Ca is concentrated in the top part of the sample. In the case of the partially filled pores, most calcite appears as pore-lining crystals (Fig. 8).

Sample III

The sample HU values are characterized by a slightly negatively skewed, multimodal leptokurtic distribution (MD: 2510.27, STD:741.46, SK: -1.75, K:2.55), with multipeaks at the lower and upper ends (first one at 327 HU, reflecting the lower density component). The largest peak is at 2757 HU, close to the sample mean, with another peak at the right shoulder at 3188 HU reflecting the dominance of the highest density components in the sample (Fig. 9). Multiple peaks on the histogram indicate the presence of multiple rock-forming components with significantly different proportions than in the previous sample.

There are 5 overlapping groups characterized by slightly different densities with a wide distribution between 0 and 3867 HU in the sample. The first group (A) is <490 HU. The group B has a wider range between 122 to 2350 HU. When we check the RFCs related to these intervals on the 3D brick from the CT scan, they appear to form a network of isolated and interconnected spherical and elongated tubular structures (Fig. 10/1). In our view, they correspond to various types of pores, moldic pores appearing as spherical elongated and vuggy pores appearing as tubular structures.

The third one (group C in Fig. 10/3) corresponds to the interquartile area on the boxplot of Fig. 9 indicating that this group gives a major part of the rock-forming components. The group C is characterized by two overlapping modes (C1, C2) referring to the presence of two dominant components with lower (group C1: 2163–3193 HU) and higher densities (group C2: 2757 HU and 3208 HU).

The yellow-colour RFC with values of the group C on the CT brick corresponds to the upper light-grey area of the original sample (Fig. 10/3) and represents the carbonate matrix consisted of lower density calcitic micrite and higher density dolomitic micrite.

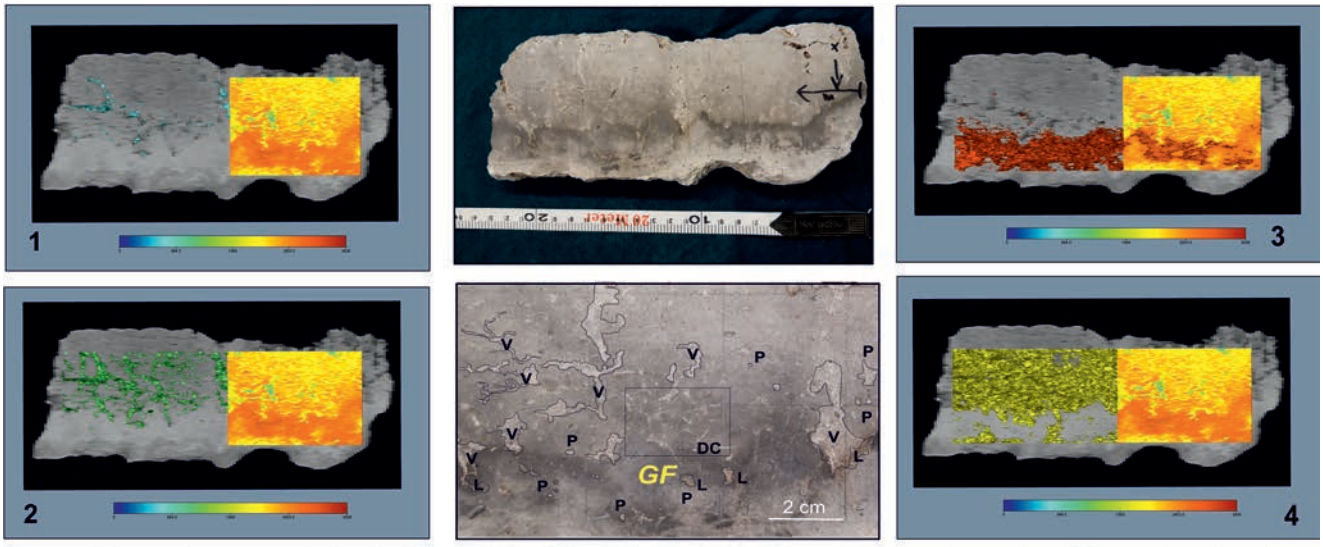

Fig. 10. The visual appearance of identified subpopulations (A, B, C1, C2, D) on the CT block of sample III (1: empty pores (A), 2: calcite filled pores (B), 3. calcitic and dolomitic matrix (C1, C2), 4: limonite and manganese saturated micrite (D).

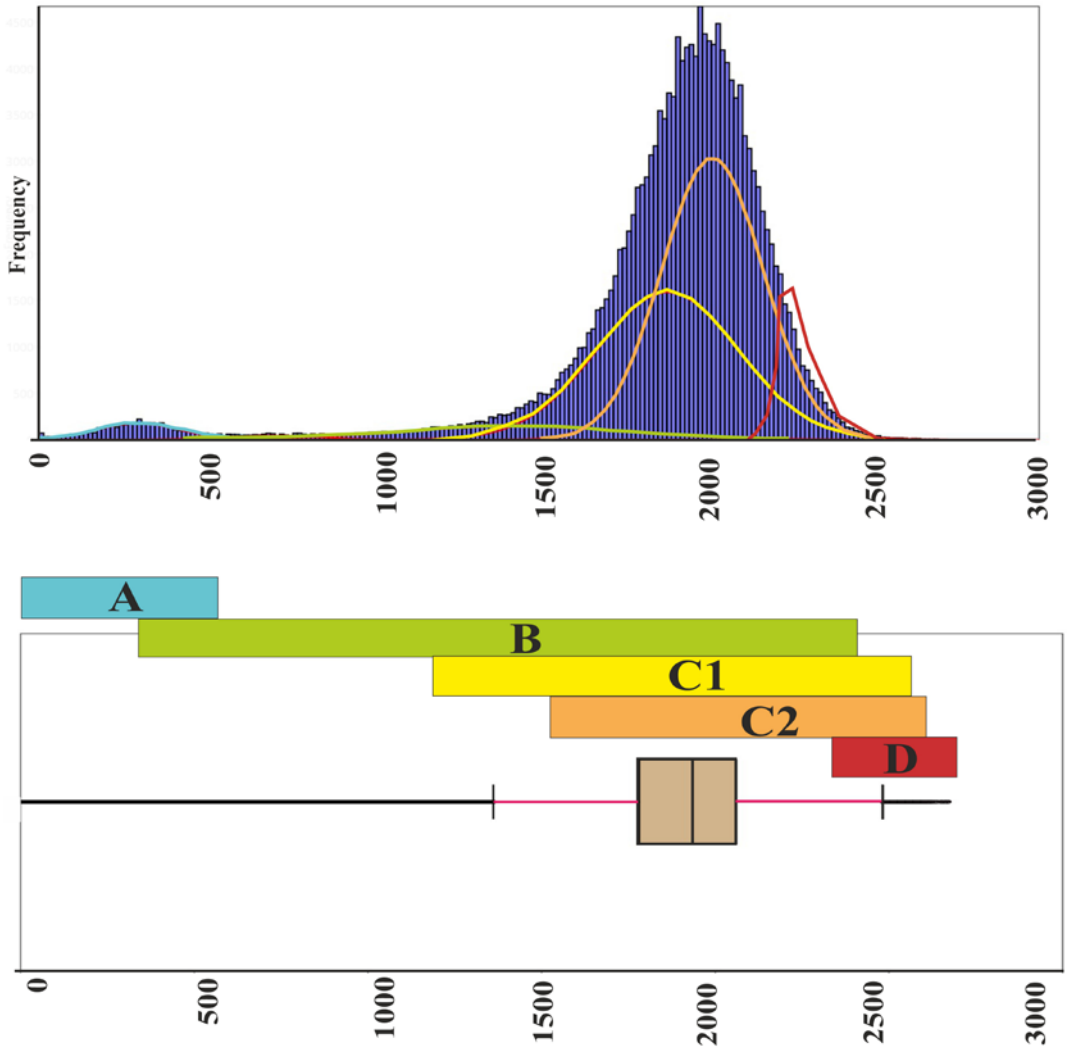

Fig. 11. Statistical characteristics of sample IV and revealed subpopulations (A, B, C1, C2, D) represented by overlapping normal distribution curves on the frequency histogram.

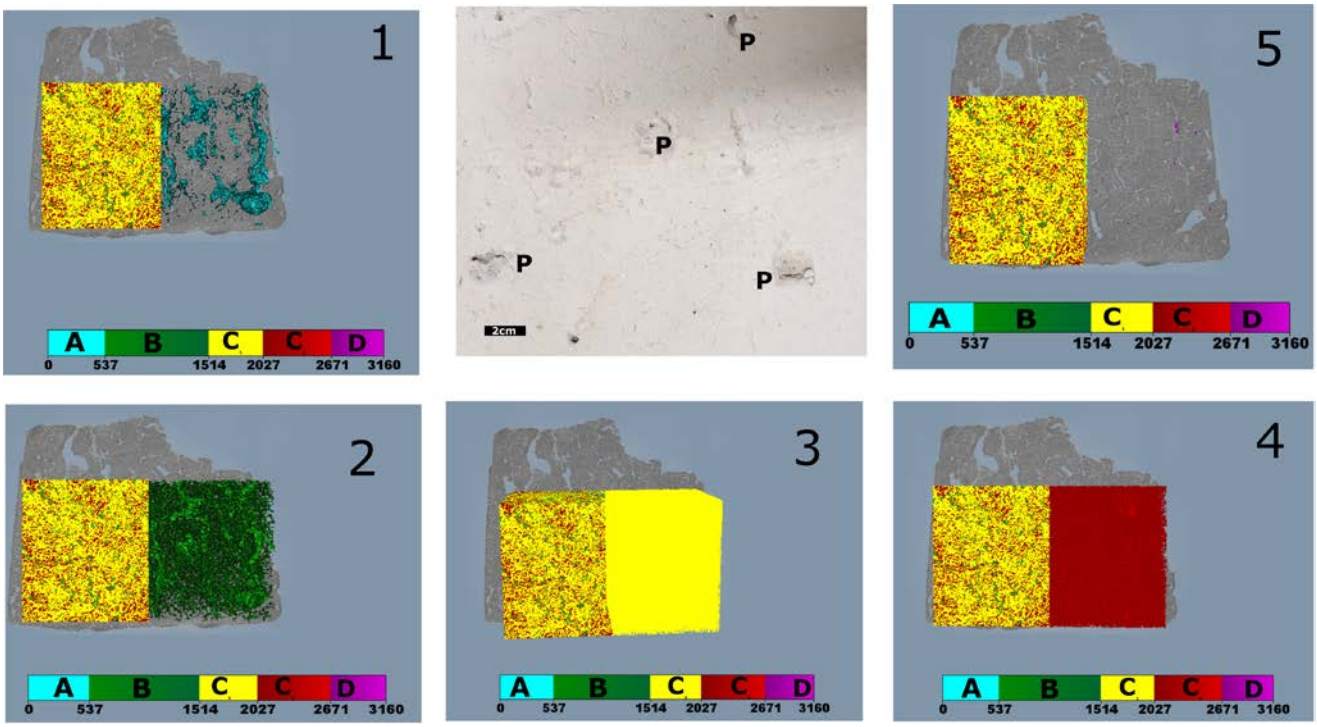

Fig. 12. The visual appearance of defined HU intervals (A, B, C1, C2, D) on the CT bricks of sample IV (1: empty pores (A), 2: filled pores (B), 3: matrix of dominantly calcitic micrite (C1), 4: matrix of dominantly dolomitic micrite (C2), 5: Limonite and manganese saturated micrite (D)).

The sample largest density values are found in the last group (D) (3088–3388 HU). We can expand the top border of this range to the sample greatest value (3938 HU). While the group D overlaps with the group C, which we regarded as the matrix, this group must also represent a component of the matrix, implying the presence of a higher density substance. When the group D is visualized on the CT brick (Fig. 10/4), there is a perfect match with the dark grey-brownish bottom part of the original sample representing a geochemical front (GF) of the limonite, saturated dominantly a dolomitic matrix just like in the sample II.\

Sample IV, member Cs-4.

The last member of the profile is characterized by a bimodal (MD: 1934, STD:355, SK: -1.16E+04, K:720), negatively skewed and highly peaked distribution, indicating low density (292 HU) and dominance of a high-density component (1985 HU), close to the sample mean (Fig. 11).

Based on the mixture analysis results (Fig. 11), also 5 overlapping groups with a density between 0 and 3160 HU could be distinguished. The group A is characterized by values <537 HU. The group B has a broader distribution between 336 and 1907 HU. Visualizing the RFCs, regarding these intervals on the CT brick, they represent a network of interconnected spherical and tubular structures that can be interpreted to be pores, just like in the case of the previous samples (Fig. 12/1, 2). There are different types of pores regarding their shape, also clearly visible in the thin section: molds and vugs (Figs. 12, 13).

In a thin section, pores appear in various states: empty pores belong to the first group A, partially filled with crystals lining over the border of the pore during early diagenesis, almost fulfilled with crystals during the early diagenesis, based on the pore water chemistry. Therefore, the group B extends widely from low (almost empty pores) to higher density (filled or partially filled with calcite).

The next group C can be divided into two main subgroups (C1, C2), the first one (C1) ranging from 1328 to

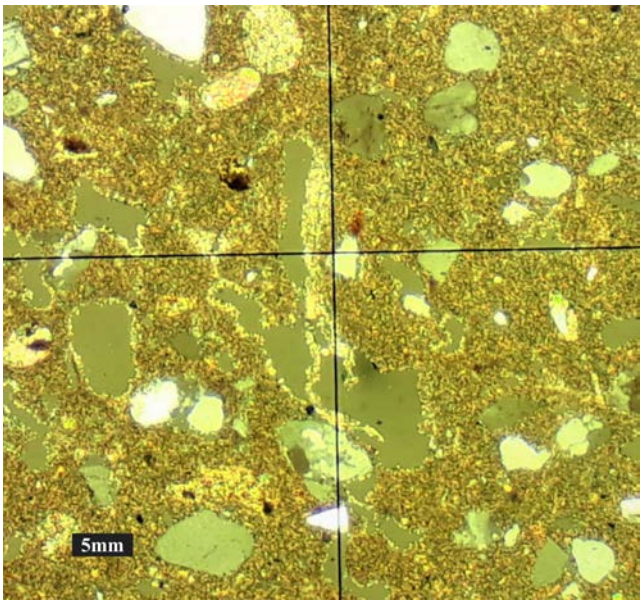

Fig. 13. The thin section from sample IV shows empty pores and filled/partially filled pores, matrix. (30 x magnification, Xpl).

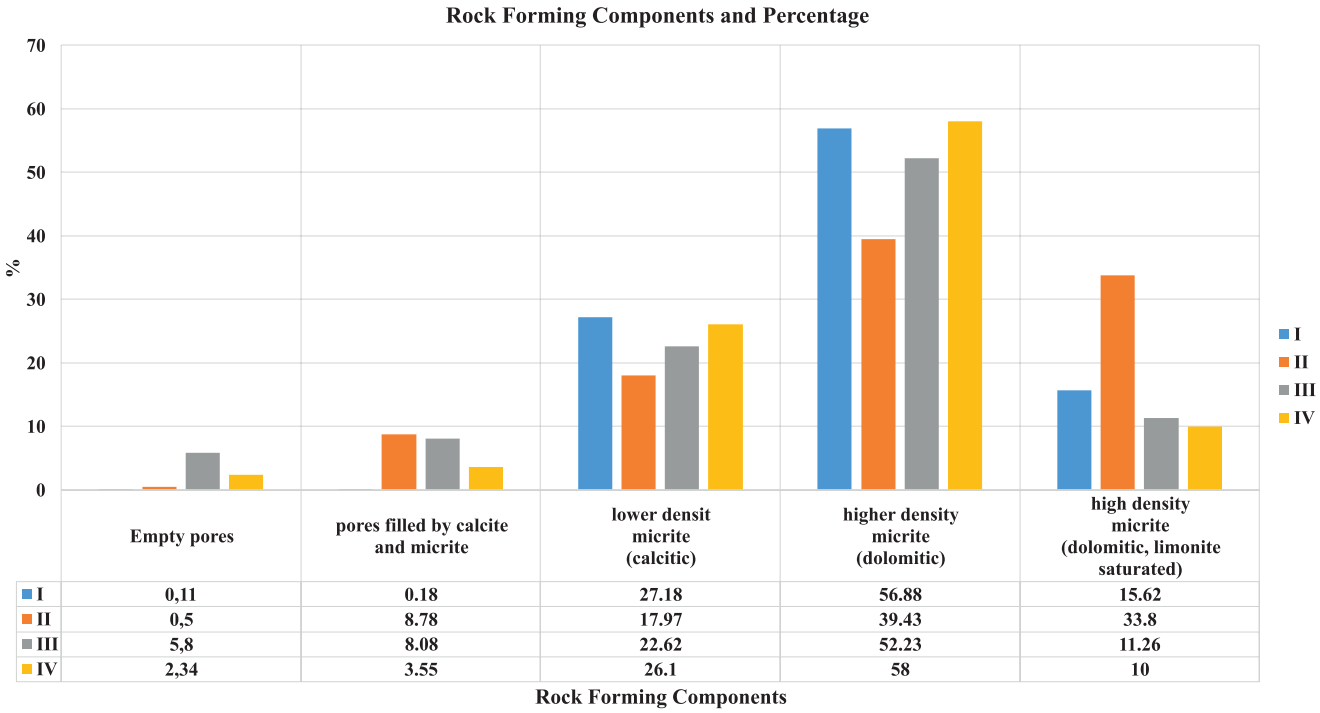

Fig. 14. Proportions of major RFCs determined by CT analysis.

2261 HU (mean: 1794 HU). As this interval partly overlaps the group B which we interpreted as pores filled with calcite crystals, the group C1 must represent the matrix with a larger proportion of a calcite micrite too. The whole higher density part overlapped with the last interval. Most RFCs were found in the groups C1 and C2. The group D distributed between 1669 to 3160 HU. On the boxplot, the interquartile area and both whiskers represent the groups C1 and C2. Thus, the RFCs of these groups are probably a calcitic micrite mud and a dolomitic micrite mud. As there is a large overlap between these groups; some of the dolomites may be assumed to have precipitated into the pores from a high magnesium content in porewater, in addition to development of a dolomite mud from a calcite mud by entering Mg^{++} to mineral crystals.

The last group of this sample is the group D with values ranging between 2560 to 3160 HU, which corresponds to the highest density components such as Fe^{+2}, Fe^{+3}, Mn^{+2} and Mg^{+2}, transported by groundwater fluctuation or dissolved by meteorite water during surface runoff.

Estimated proportions of RFCs

Based on our calculations, pores give ca. 0.29% of the total volume in the sample I. The proportion of empty pores is negligible around ~0.11%. According to Molnár (1981, 1983), most of the pores are vugs, intergranular and moldic ones. All types are observed in the sample (Fig. 4). As it was seen in our CT blocks, vugs corresponding to roots of the former vegetation appear in various forms and orientation. A concentration of these features is generally highest in the member Cs-1 and much lower in the member Cs-2. Their proportion is minimal in the transitional zone of the two members. Looking at the photos depicting the original samples (Fig. 4), the mentioned features correspond to the dark-grey and dark-brown areas, representing dominantly pores infilled with limonite and manganese saturated micrite. These minerals infilling pores precipitated during seasonal fluctuations of the groundwater. In the studied volume, 90% represents a matrix, 27.18% of which is composed dominantly of the lower density calcitic micrite and 56.88% is given by the higher density dolomitic and limonite saturated micrite (Fig. 14), with a shear dominance of the highest density micrite (15.62% on the average). It must be kept in mind that the densest part of the matrix is composed of high-density minerals (dolomite, limonite), plus a larger proportion of higher density clastics (quartz, feldspars, clays).

Based on the results of detailed XRD investigations (Molnár *et al.*, 1976; Molnár, 1991, 2015), both members Cs-1 and Cs-2 are classified as dolomitic limestone or mud-supported wackestone according to Dunham (1962). Although a general chemical composition of members Cs-1 and Cs-2 is quite similar (74–77% $CaCO_3$ and 19.4–22.3% $CaMg(CO_3)_2$), previously published results of thin-section analyses of both members highlighted significant variations in the proportion as well as the mineralogical composition of the individual matrix components (Molnár *et al.*, 1976; Molnár, 1991, 2015). In the member Cs-1, 58–67% of the matrix is a micrite, composed of anhedral calcite crystals (Molnár *et al.*, 1976; Molnár, 1991, 2015). The proportion of clastic particles (quartz, feldspar, clay) is relatively high (21–24%), while dolomite patches are subordinate, appearing in a size of <1 mm. In the member Cs-2 with a much

more uniform texture than the member Cs-1, a proportion of the micritic matrix is also higher (75–78%), dominantly composed of anhedral calcite crystals and subordinately euhedral dolomite. Clastics are present but in much lower content of 13–15% (Molnár *et al*., 1976; Molnár, 1991, 2015). This is corroborated by our estimated proportions of RFCs in the sample I using the CT data. The calcitic micrite is 27.18% (Fig. 14) but our data are a sum of values for the entire Cs-1 and Cs-2 complex. Most likely, higher proportions of the matrix in our data must be representative of the Cs-2 member the sample I.

In the samples of the member Cs-3 ("pecsmeg" samples II and III) a proportion of the pores is much higher (9.28% in the sample II and 13.88% in the sample III, respectively) than in members Cs-1 and Cs-2 (Fig. 14). It is interesting to note that the sample II is more compact with a smaller number of pores compared to the sample III. So, most of the pores are calcite sparite or micrite filled, which represent around 8.78% and 8.08% in the samples II and III, respectively (Fig. 14). The latter is developed by unconsolidated mud filling only partially the empty shells or pores. Gas pores are usually isometric in the unconsolidated saturated carbonate mud, however they are distorted during desiccation and lithification (Choquette and Pray, 1970). Macropores are more abundant here than in the members Cs-1 and Cs-2. Macropores are the most diverse in this member as well (Figs. 7, 8, 10). Desiccation cracks, sheet cracks, open and closed gas pores, root pores appear cutting through the laminae. The ratio of intergranular pores is negligible. So-called sheltered pores also turn up (Molnár *et al*., 1976; Molnár, 1991, 2015). The limonite saturated matrix is up to 11.26% in the sample III compared with 33.8% in the sample II, which is higher than in the sample I. The member Cs-3 ("pecsmeg" samples II and III) is a mud-supported wackestone with a highly complex texture recorded by thin-section analyses (Molnár *et al*., 1976; Molnár, 1991, 2015). As reported by Molnár *et al.* (1976), the dominant component is a micrite (76–82%), the proportion of which is slightly higher than that of the member Cs-2. When compared with the underlying members (Cs-1, Cs-2), the member Cs-3 has ca. 10% lower $CaCO_3$ content of 65.1–66.5% and ca.5–7% higher $CaMg(CO_3)_2$ content of 26.5–32.1% (Molnár *et al*., 1976; Molnár, 1991, 2015).

Based on our data, the proportion of the lower density calcitic micrite is 17.97 % in the sample II and 22.62% in the sample III (Fig. 14). Higher density dolomitic micrite is present in higher amounts (39.43% in the sample II and ~52.23% in the sample III). The proportion of quartz and feldspars is the lowest in this part of the profile (9.0–9.5%) based on thin-section data (Molnár *et al*., 1976; Molnár, 1991, 2015).

The sample IV (member Cs-4), based on the results of detailed XRD investigations (chalk) is dolomite. Based on thin-section data, a proportion of $CaCO_3$ and $CaMg(CO_3)_2$ is highly variable with values ranging between 36.1–65.6% of the former and 34.8–59% of the latter (Molnár *et al*., 1976; Molnár, 1991, 2015). According to our results, the dominant matrix is a dolomitic micrite with ~58% while the calcitic micrite is ~26.1% in the sample (Fig. 14). As the rock is described as a dolomite mud, our result confirmed a dominance of higher density mineral dolomite in the matrix.

In the member Cs-4, the micrite ratio is reduced to 49–60% compared to the members Cs-1, Cs-2 and Cs-3 (Fig. 14). There is an increase in the proportion of quartz and feldspars to 16–23%. Lithic components are reduced in size (0.02–0.06 mm). The proportion of carbonate lithics also increases (6.5–8.5%). These clasts are intraclasts rather than exoclasts, having been ripped off a bottom of the lake by winds during a complete desiccation of the lakebed.

Pores filling sparite and microsparites are completely lacking here. The major pore types are desiccation, gas and root ones. Fossil Chara oogonia and gastropod shells also turn up here. which indicates that these samples could have the same precipitation environment, approximately similar in physiochemical or biological conditions. Based on our HU values (Fig. 14), empty pores are ~2.34%. Pores filled or partially filled with Ca^{+2} are ~3.55%, while the higher density mud saturation limonite is up to ~10% in the sample IV.

CONCLUDING REMARKS

Understanding and documenting the heterogeneity and textural properties of carbonates using the CT data are straightforward and more objective than thin-section analysis based estimations. The quantitative information provided by thin sections is limited to the areas of the studied sample where subsamples were selectively taken for such investigations. In addition, estimations are rather subjective. Several different RFCs are present within a single grid cell, so correct filtering of the individual components and estimation of their proportions in the grid is not without bias. The CT analysis however provides us quantitative data in 3D at both the scale of the entire sample and a resolution defined by dimensions of the voxels at the micro-scale. The quantitative data expressed in the HU correlates with the density of the RFCs. Thus, its statistical properties also record information on their textural heterogeneity.

Previous studies of freshwater carbonates of the DTI in central Hungary have clearly defined the major textural components as calcite and dolomitic micrite, calcite sparite, carbonate clastics, quartz, feldspars and limonite (Molnár, 1961, 1970, 1980, 1983, 1985, 1991, 1996; Mucsi, 1963; Molnár and Murvai, 1976; Molnár and Szónoky, 1976; Molnár *et al.,* 1995). All mentioned minerals are characterized by different densities (calcite 2.71 g/cm^3, limestone 2.711 g/cm^3, dolomite 2.84 g/cm^3 and limonite 2.7–4.3 g/cm^3) which is also expressed in the CT-based HU values. As the studied rocks represent a pool of the RFCs, in this pioneering work we adopted mixture analysis as a non-hierarchical clustering method for the segmentation of each RFCs using the CT data. We have found only two references that reported the CT-based density data for carbonates: limestone (2765 HU; Bolliger *et al*., 2009), secondary formed marine dolomite in claystone of

the Permian Boda Claystone Formation (3300–3600 HU; Abutaha *et al*., 2021). These could have been used only as tentative guidelines in our work as the density values are highly dependent on the complexity of the studied rock sample, i.e. types, proportion and collective presence of the RFCs. This complexity is also recorded in the overlap of distribution curves of each meaningful sub-populations determined by mixture analysis of the CT data in our work. So, setting up discrete boundaries for the RFCs is not easy and that is why the CT-based density data is reported as intervals in our work in addition to mean and 2 STD.

Knowing the original volume of the studied and filtered subsamples, the percentage of each identified rock-forming component (e.g., calcitic matrix, filled pores, etc.) can also be estimated. The proportions of each rock-forming component calculated using the CT data can be compared to those defined by multiple thin section analyses on subsamples taken from selected parts of the studied sample. In light of our results providing a better estimate on the proportions of the RFCs for the entire volume of the sample than thin sections, the nomenclature of the rocks must be reconsidered. XRD analysis provides us only semi-quantitative data on the presence and the proportion of rock-forming minerals. In 1960s and 1970s, technical limitations in the XRD analysis hampered the estimation of the exact proportions of each identified mineral. In older studies as those of Molnár (1961, 1970, 1980, 1983, 1985, 1991, 1996) applying the XRD for the identification of rock-forming minerals in freshwater carbonate samples of the DTI, intensity of mineral peaks was considered for naming the studied rocks of each member of the Csólyospálos profile. According to our findings in samples where the proportion of the calcitic micrite is greater than that of the denser dolomitic, limonite saturated micrite the samples can be determined as a dolomitic limestone. Contrary, where the densest components (dolomitic, limonite saturates micrite) are dominant, the name dolomite is adequate.

Acknowledgments

The authors are grateful to reviewers for their critical comments helping to improve the original manuscript. This work has been partially supported by NSF Grant K129265, and grants by the European Union, and the State of Hungary, co-financed by the European Regional Development Fund in the projects of GINOP-2.3.2-15-2016-00009 'ICER'" as well as the Ministry of Human Capacities, Hungary Grant 20391-3/2018/FEKUSTRAT.

REFERENCES

Abutaha, S.M., Geiger, J., Gulyás, S., Fedor, F., 2021. Evaluation of 3D small-scale lithological heterogeneities and pore distribution of the Boda Claystone Formation using X-ray computed tomography images (CT). Geologia Croatica 74 (3), 305–318. doi: 10.4154/gc.2021.17

Akaike, H., 1974. A new look at statistical model identification. IEEE 19/6, 716–723. doi: 10.1109/TAC.1974.1100705

Bender, M.L., Lorens R.B., Williams, D.F., 1975. Sodium, Magnesium And Strontium in the tests of planktonic foraminifera. Micropaleontology 21 (4), 448–459.

Bolliger, S.A., Oesterhelweg, L., Spendlove, D., Ross, S., Thali, M.J., 2009. Is Differentiation of Frequently Encountered Foreign Bodies in Corpses Possible by Hounsfield Density Measurement? Journal of Forensic Sciences 54 (5), 1119–1122.

Chen, Y., Shen, A., Pan, L., Zhang, J., Wang, X., 2017. Features, origin and distribution of microbial dolomite reservoirs: a case study of 4th member of Sinian Dengying Formation in Sichuan Basin, SW China. Petroleum exploration and development 44 (5), 745–757.

Choquette, P.W., Pray, L.C., 1970. Geologic nomenclature and classification of porosity in sedimentary carbonates. American Association of Petroleum Geologists Bulletin 54, 207–250.

Cnudde, V., Masschaele, B., Dierick, M., Vlassenbroeck, J., Van Hoorebeke, L., Jacobes, P., 2006. Recent progress in X-ray ct as a geosciences tool. Applied geochemistry 21 (5), 826–832. doi:10.1016/j.apgeochem.2006.02.010

De Boever, W., Derluyna, H., Van Loob, D., Van Hoorebekec, L., Cnudde, V., 2015. Data-fusion of high-resolution X-ray CT, SEM and EDS for 3D and pseudo-3D chemical and structural characterization of sandstone. Micron 74, 15–21. doi: 10.1016/j.micron.2015.04.003.

Dempster, A.P., Laird, N.M., Rubin, D.B., 1977. Maximum likelihood from incomplete data via the EM algorithm, Journal of Royal Statistical Society 39 (1), 1–38.

Fang, Y., Xu, H., 2019. A new approach to quantify the ordering state of Protodolomite using XRD, TEM, and Z-contrast imaging. Journal of sedimentary research 89 (6), 537–551. doi:10.2110/jsr.2019.29

Földes, T., Árgyelán, G.B., Kiss, B., Repa, I., Bogner, P., 2004. Application of medical Computer Tomography measurements to 3D reservoir characterization. Acta geologica hungarica 47(1), 63–73. doi: 10.1556/AGeol.47.2004.1.5

Gaines, A.M., 1977. Protodolomite redefined. Journal of sedimentay petrology 47/2, 543–546.

Hammer, Ø., Harper, D.A.T., Ryan, P.D., 2001. PAST : Paleontological Statistics software package for education and data analysis, 275 pp.

Hicks, P.J., Ram Narayanan, K., Deans, H.A., 1994. An experimental study of miscible displacements in heterogeneous carbonate cores using X-ray CT. SPE Formation Evaluation 9 (01), 55–60.

Jenei, M., Gulyás, S., Sümegi, P., Molnár, M., 2007. Holocene Lacustrine Carbonate Formation: old ideas in the light of new radiocarbon data from a single site in central Hungary. Radiocarbon 49(2), 1017–1021.

Kenter, J.A.M., 1989. Applications of Computerized Tomography in Sedimentology. Marine geotechnology 8 (3), 201–211. doi: 10.1080/10641

Markussen, Ø., Dypvik, H., Hammer, E., Long, H., Hammer, Ø., 2019. 3D characterization of porosity and authigenic cementation in Triassic Conglomerates/Arenites in the Edvard Grieg field using 3D Micro-CT Imaging. 2019. Marine and Petroleum Geology 99, 265–281. doi: 10.1016/j.marpetgeo.2018.10.015.

Maurício, A., Pereira, M.F., Rocha, C., Figueiredo, C., Marques, J.M., 2017. X-ray Micro-CT study of Cabeço De Vide Serpentinites and carbonate rock samples: a preliminary approach. Procedia earth and planetary science 17, 952–955. doi:10.1016/j.proeps.2017.01.034.

Mihältz, I., 1947. A Duna-Tisza – csatorna geológiai viszonyainak tanulmányozása – A Duna-Tisza – csatorna, Földm. Min. Kiadványa, Budapest, 3–12 (in Hungarian).

Mihältz, I., 1953. A Duna-Tisza köze déki részének földtani felvétele – MÁFI évi jelentése az 1950. évről, 113–148 (in Hungarian).

Mihältz, I., Faragó, M., 1946. A Duna-Tisza közi édesvízi mészkőképződmények – Az Aéfölf Tudományos Intézet 1944–45. évi Évkönyve 1. Szeged, 371–384 (in Hungarian).

Molnár, B., 1961. A Duna-Tisza közi eolikus rétegek felszini és felszin alatti kiterjedése – Földtani Közlöny 91.3, 294–297 (in Hungarian).

Molnár, B., 1970. On the origin and hydrogeology of natron lakes in the southern great Hugarian palin, Móra Ferenc Múzeum Évkönyve/1, 65–76.

Molnár, B., 1980. Hiperszalin dolomitképződés a Duna-Tisza közen – Földtani Közlöny 100.1, 45–64 (in Hungarian).

Molnár, B., 1981. Szeimentológia I. k. – JATE TTK egzetemi jegyzet, Szeged. 298 p. (in Hungarian).

Molnár, B., 1983. A Duna-Tisza közi tavak keletkezése, fejlődéstörténete és hasznositása – Akadémiai Doktori Értekezés, Szeged, 156P. (in Hungarian).

Molnár, B., 1985. Földtani kutatások a Kiskunsági Nemzeti Parkban – in Tóth K. (szerk.) Tudományos kutatások a kiskunsági Nemzeti Parkban 1975–1984, OKHT kaidása, 29–58 (in Hungarian).

Molnár, B., 1988. Quaternary geohistory of the Hungarian part of of the Danube-Tisza Interfluve. Proceedings of geoinstitute 21, 61–78, Belgrade.

Molnár, B., 1991. Modern lacustrine Calcite, Dolomite and Magnesite Formation in Hungary. Publication of the department of Quaternary geology, University of Turku, 1–22.

Molnár, B., 1996. A szegedi Fehér-tó keletkezése és vízföldtana. Hidrológiai Közlöny 76. 5., 266–271 (in Hungarian).

Molnár, B., 2000. A Duna-Tisza köz délnyugati részének negyedidőszak végi földtani fejlődéstörténete. In: Fábian, Sz.Á. – Tóth J. (Eds.), Geokronológia és domborzati fejlődés, Pécsi Tud. Egyetem Term. Tud. Kar Földrajzi Int. Kiadványa, Pécs, 101–121 (in Hungarian).

Molnár, B., 2015. A Kiskunsági nemzeti park – Földtana és vízföldtana, JatePress, 523 pp.

Molnár, B., Geiger, J., 1981. Homogénnek látszó rétegsorok tagoláai lehetősége zedimentológiai, őslénytani és matematikai módszerek kombinált alalmazásával – Földtani köz. 111. 2., 238–257.

Molnár, B., Murvai, M.I., 1976. A kisunsági Nemzeti Park fülöphaázi szikes tanvainak kialakulása és földtani története – Hidrológiai közlöny 56. 2, 67–77.

Molnár, B., Szónoky, M., 1976. On the Origin and Geohistorical Evolution of the Natron lakes of the Bugac Region – Móra F. Múzeum Évkönyve, Szeged 1974/75. 257–270.

Molnár, B., Murvai, M.I., Hegyi-Pakó, J., 1976. Recent lacustrain Dolomite formation in the great Hungarian plain. Acta geologica academiae socientiarum Hungaricae, Tumus 20 (3–4), 179–198.

Molnár, B., Hum, L., Fényes, J., 1995. Investigation of modern geological processes in Holocene lacustrine carbonates in the Danube-Tisza Interfluve – Hungary. Acta mineralogica-petrographica, Szeged, XXXVI, 73–87.

Mucsi, M., 1963. Finomrétegtani visózsgálatok a kisunsági édesvizi karbonátképződményekben, Földtani közlöny. Bulletin of the Hungarrian Geological Society 93/3, 373–386.

Müller, G., 1970. "High-Magnesian Calcite and protodolomite in lake Balaton (Hungary) sediments. Nature 226, 749–750.

Müller, G., Irion, G., Förstner, U., 1972. Formation and diagenesis of inorganic Ca-Mg carbonates in the lacustrine environment. Die naturwissenschaften 59 (4), 158–164.

Müller, G., Wagner, F., 1978. Holocene carbonate evolution in Lkae Balaton (Hungary): a response to climate and impact of man. special publication int. ass. sediment., 2, 57–81.

Sümegi, P., Molnár, D., Sávai, Sz., Náfrádi, K., Novák, Z., Szelepcsényi, Z., Törőcsik, T., 2015a. First Radiocarbon dated paleoecological data from the freshwater carbonates of the danube-tisza interfluve. Open geosciences 7(1), 40–52. doi: 10.1515/geo-2015-0003

Sümegi, P., Náfrádi, K., 2015b. A radiocarbon-dated cave sequence and the Pleistocene/ Holocene transition in Hungary. Open geosciences (1), 783–798. doi:10.1515/geo-2015-0051.

Tullner, T., Cserny, T., 2003. New Aspects of Lake-Level Changes: Lake Balaton, Hungary. Acta Geologica Hungarica 46 (2), 215–238.

Wilding, M., Lesher, C. E., Shields, K., 2005. Applications of neutron Computed Tomography in the geosciences. Nuclear instruments and methods in physics research, section, A, 542 (1–3), 290–295. doi:10.1016/j.nima.2005.01.151